Global Nonhydrostatic Atmospheric Modeling using Spherical Centroidal Voronoi Meshes

William C. Skamarock
National Center for Atmospheric Research
Meoscale and Microscale Meteorology Laboratory

MPAS-Atmosphere Solves the Fully-Compressible Nonhydrostatic Equations

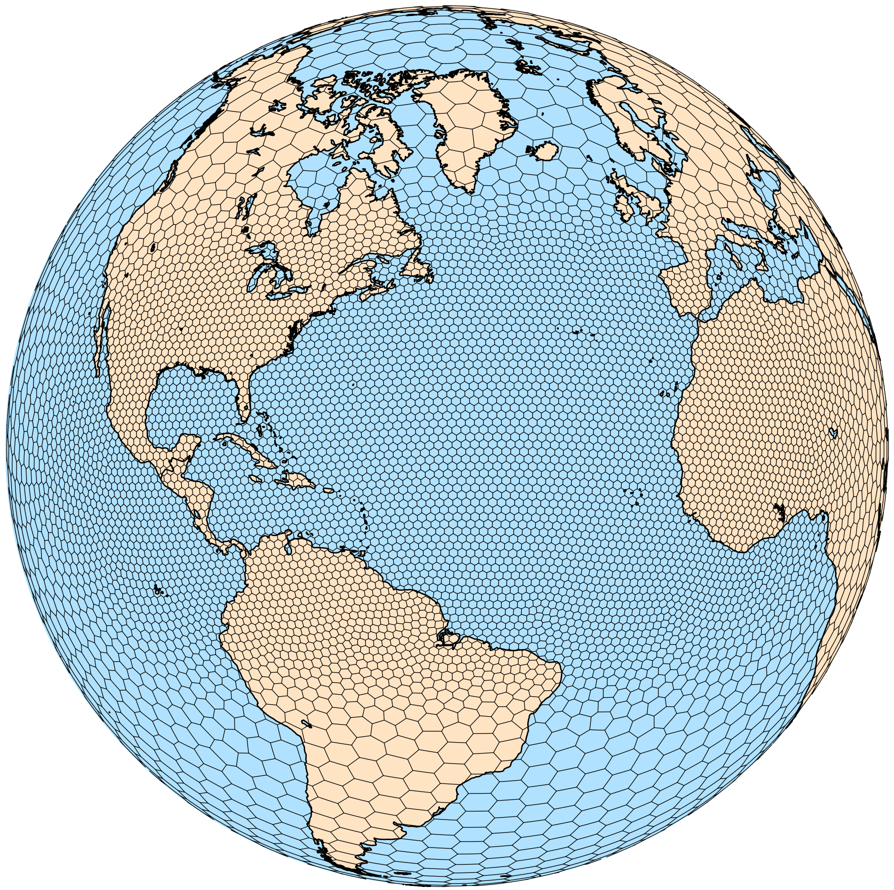

The MPAS integration scheme is similar to that in the Advanced Research WRF model

- split-explicit Runge-Kutta time integration
- C-grid spatial staggering

MPAS differs from WRF in using

- generalized height coordinate.
- spherical centroidal Voronoi mesh
- a *horizontally unstructured* mesh

MPAS
Model for Prediction Across Scales

MPAS-Atmosphere Solves the Fully-Compressible Nonhydrostatic Equations

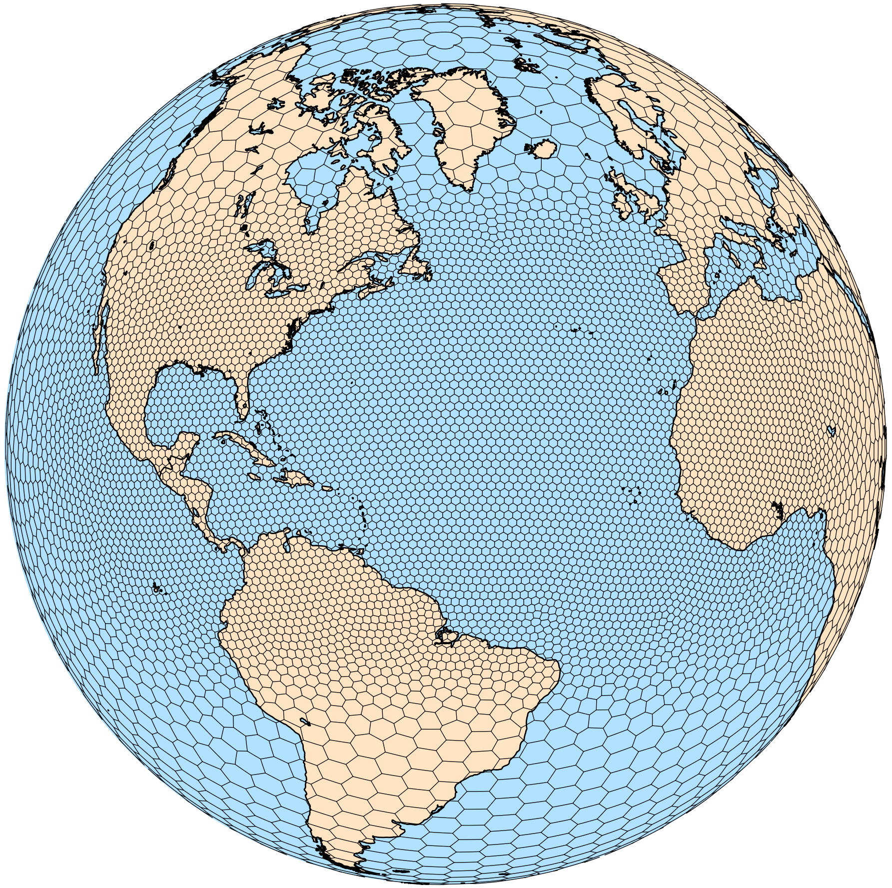

<u>Topics for Today</u>

- Centroidal Voronoi tessellation (horizontal mesh)
- High-resolution atmospheric simulations: Convection
- The C-grid problem with hexagons
- Transport on unstructured meshes
- MPAS vertical coordinate
- Strengths and weaknesses of this approach

MPAS
Model for Prediction Across Scales

MPAS-Atmosphere Solves the Fully-Compressible Nonhydrostatic Equations

<u>Unstructured spherical centroidal Voronoi Tesselation (SCVT)</u>

- Mostly *hexagons*, some pentagons and 7-sided cells
- Cell centers are at cell center-of-mass (centroidal).
- Cell edges bisect lines connecting cell centers; perpendicular.
- Uniform resolution – traditional icosahedral mesh.

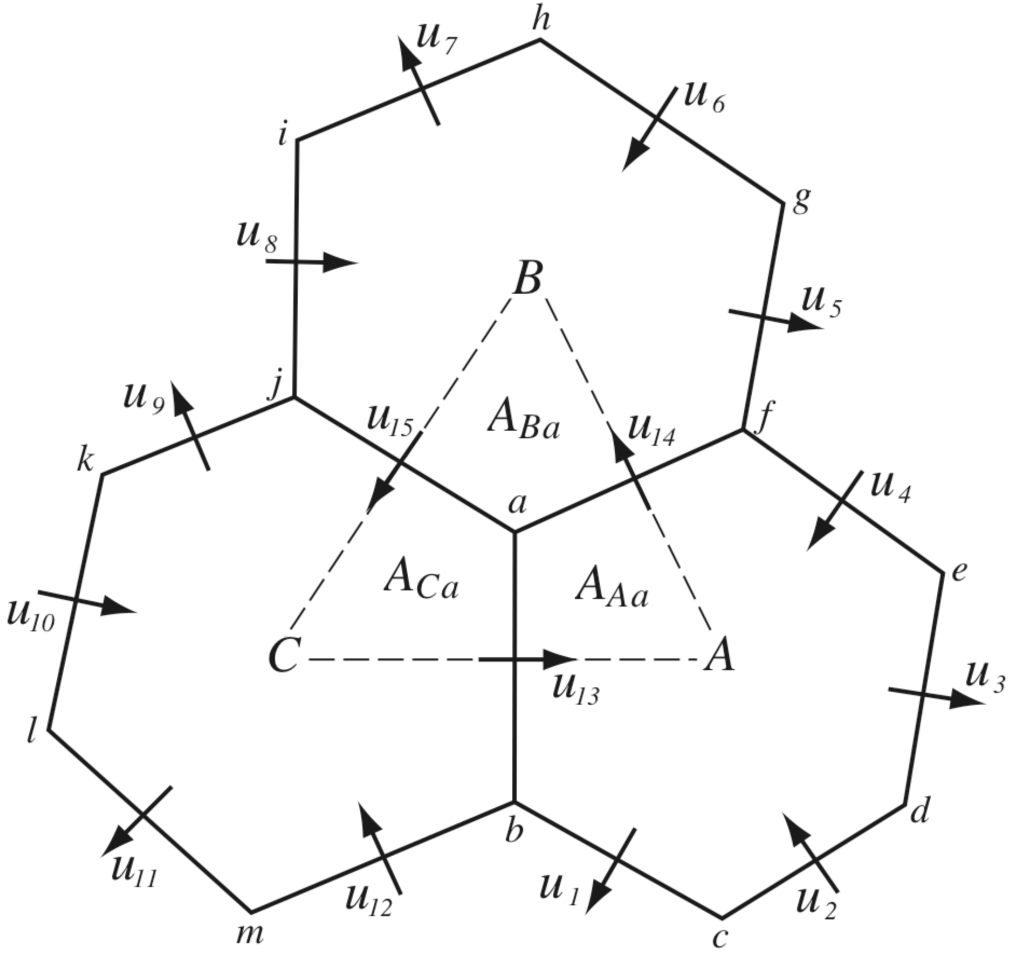

(S)CVTs are generated using Lloyd's iteration method and a user-specified density function that controls the local cell-center spacing

MPAS
Model for Prediction Across Scales

MPAS and an Interesting Mesh

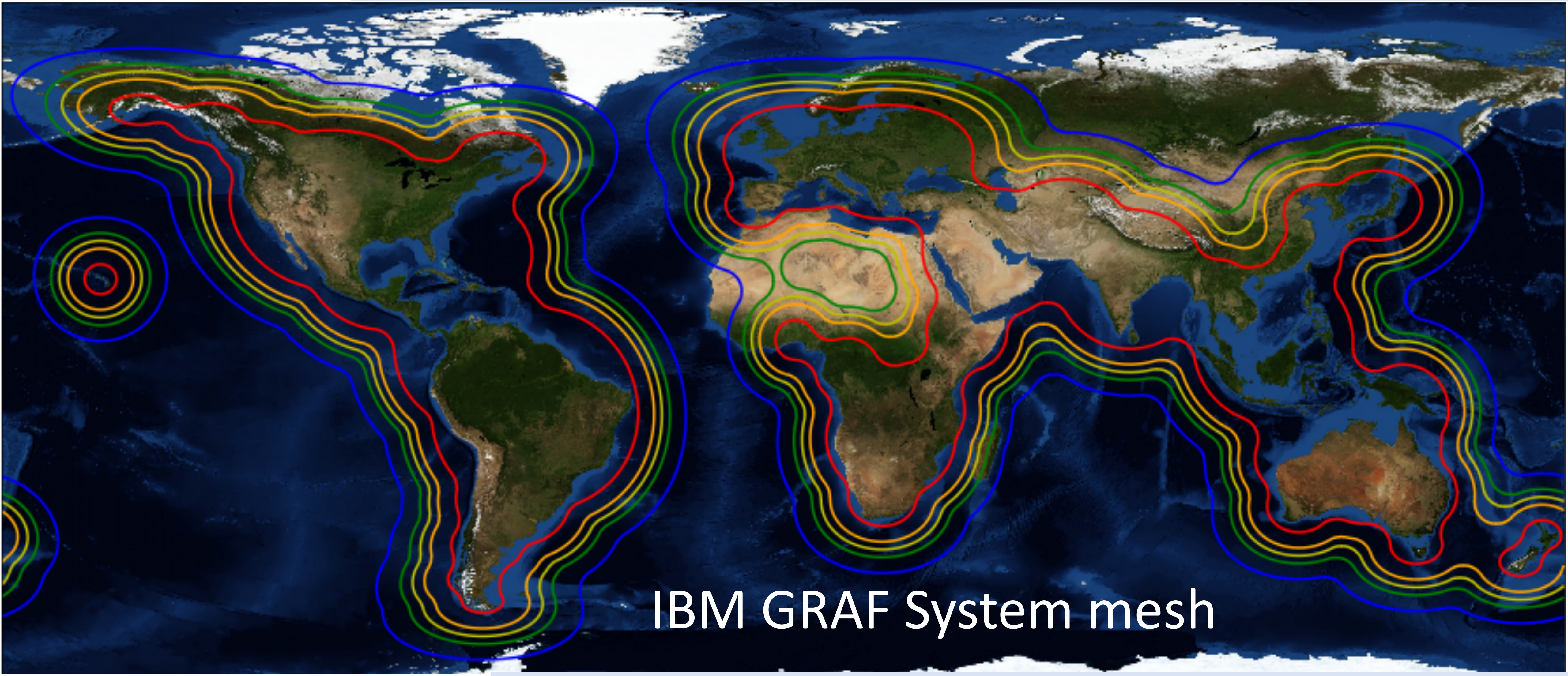

NCAR NATIONAL CENTER FOR ATMOSPHERIC RESEARCH
IBM
The Weather Company An IBM Business

IBM GRAF (Global High Resolution Forecast) System - MPAS mesh (3-15 km cell spacing)
Physics: Scale aware nTiedtke CP, YSU PBL, NOAH LSM, WSM6 microphysics

Atmospheric Convection and MPAS

MPAS was designed for global applications (e.g. SCVTs avoid pole problems)

MPAS was designed to simulate atmospheric convection with fidelity similar to state-of-the-art cloud models at

- Convection-permitting resolutions
- LES resolutions

MPAS was designed for variable resolution global and regional applications

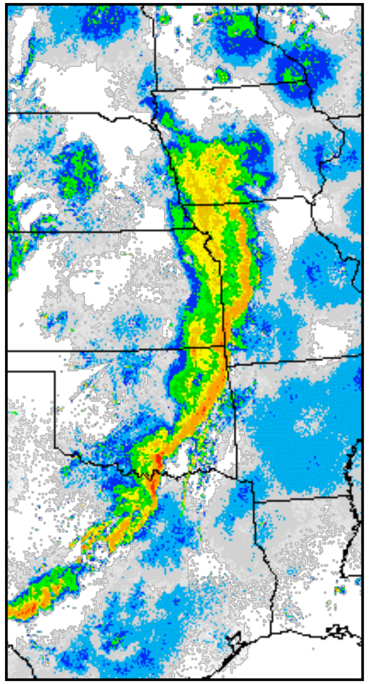

Reflectivity
NOAA SPC archive
2015-05-17 06 UTC

6 h forecast

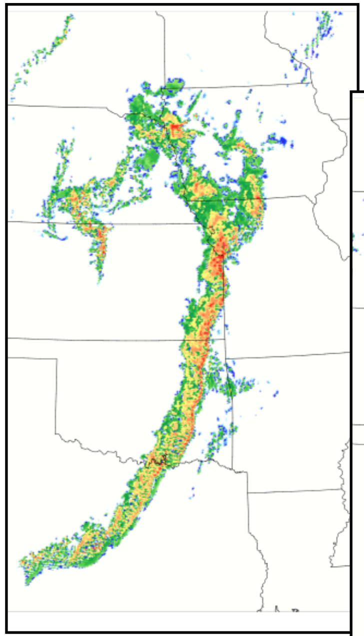

54 h forecast

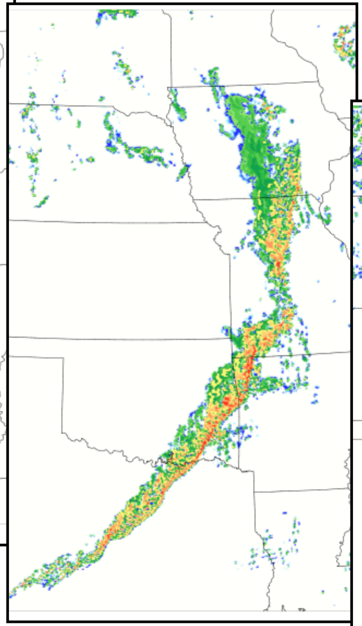

102 h forecast

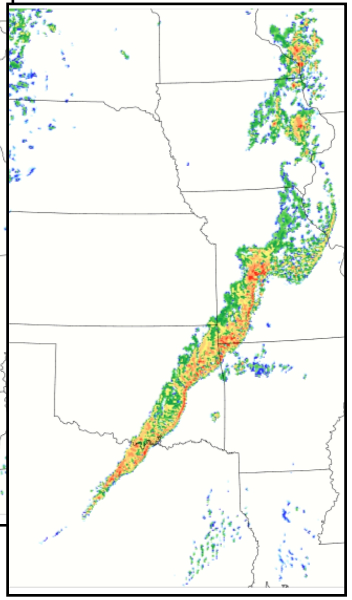

MPAS 1 km AGL reflectivity
Forecasts valid 2015-05-17 6 UTC

Spatial scales of convective updrafts

Supercells:

Reference	Type	Characteristic diameter (km) a = avg m = median s = single case	Max diameter (km)
Browning et al. (1976)	in situ and radar	5 (a)	8
Brandes (1981)	radar	11 (s)	—
Nelson (1983)	radar	∼10 (s)	—
Musil et al. (1986)	in situ	14 (s)	—
Kubesh et al. (1988)	in situ and radar	∼8 (s)	—
Dowell and Bluestein (2002)	radar	8 (s)	—

Midlatitude continental (excluding supercells):

Reference	Type	Characteristic diameter (km) a = avg m = median s = single case	Max diameter (km)
Byers and Braham (1949)	in situ	∼4	
Kyle et al. (1976)	in situ	2.8 (m)	4.6
Heymsfield and Hjelmfelt (1981)	in situ	4 (m)	6
Musil et al. (1991)	in situ	3 (a)	15
Yuter and Houze (1995)	radar	∼3 (m)	8

Spatial scales of convective updrafts

Tropical cyclones:

Reference	Type	Characteristic diameter (km) a = avg m = median s = single case	Max diameter (km)
Jorgensen et al. (1985)	in situ	1.2 (m)	7
Black et al. (1996)	radar	1 (m)	9
Eastin et al. (2005) - rainbands	in situ	1.5 (m)	3.0
Eastin et al. (2005) - eyewalls	in situ	2.0 (m)	4.0

Tropical convection (mostly maritime) (excluding tropical cyclones):

Reference	Type	Characteristic diameter (km) a = avg m = median s = single case	Max diameter (km)
LeMone and Zipser (1980)	in situ	0.9 (m)	6
Warner and McNamara (1984)	in situ	1.4 (m)	15
Jorgensen and LeMone (1989)	in situ	< 1 (m)	8
Lucas et al. (1994)	in situ	1.0 (m)	4
Igau et al. (1999)	in situ	0.8 (m)	4
Anderson et al. (2005)	in situ	1 (m)	3

Large (> 2 km) updrafts are "exceedingly rare"

Resolving Atmospheric Convection

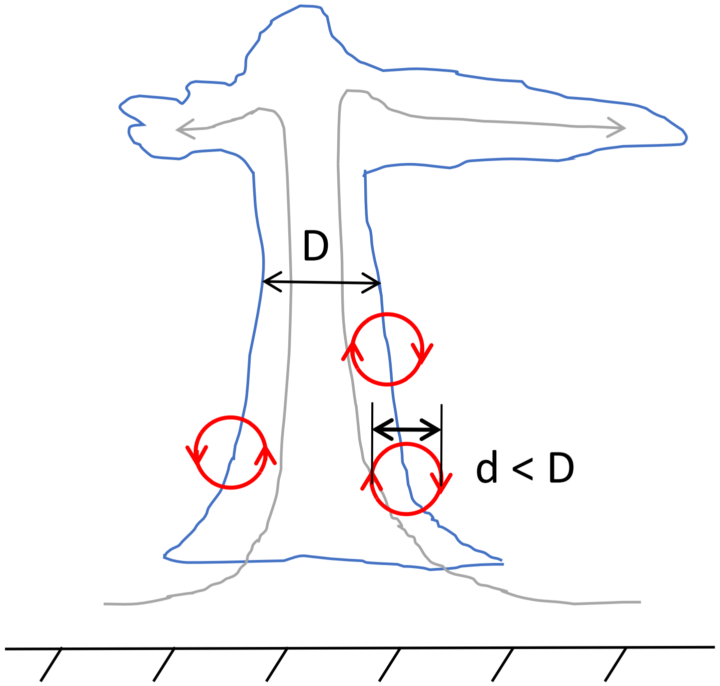

Updraft diameter: D

Eddies responsible for entrainment/detrainment: diameter d < D

Mesh spacing needed to resolve turbulent eddies: h << d, D

D: **Severe convection - 5-8 km**
Typical midlatitude cells - 2-4 km
Tropical cells - 1-2 km
Shallow convection - 0.1-1 km

Resolutions needed to *resolve* deep convection: h ~ O(100 m)

Resolutions needed to *resolve* shallow convection: h ~ O(10 m)

W spectra from global MPAS simulations

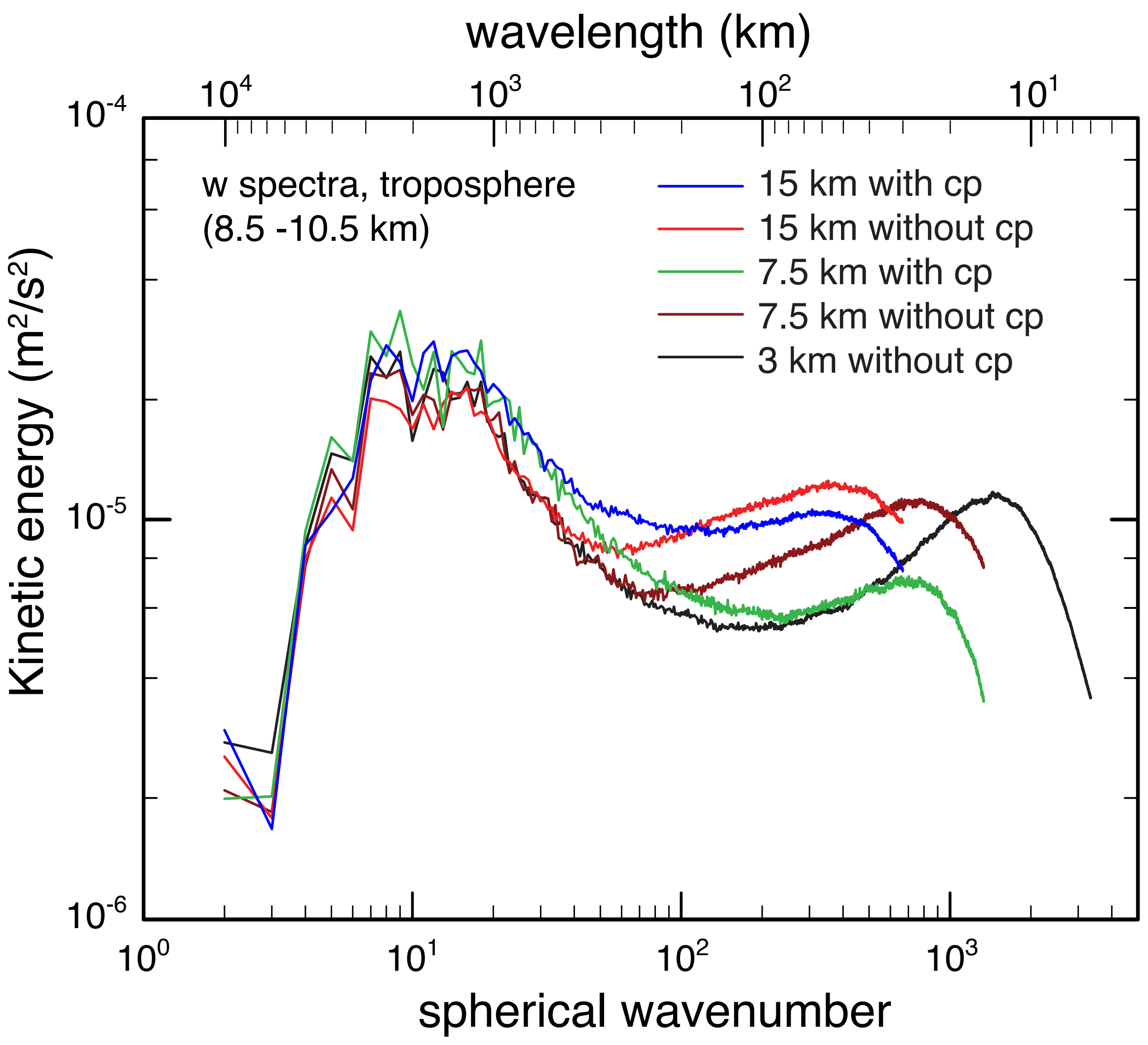

Peaks in the tails of the W spectra shift to higher wavenumbers with increasing resolution – solutions are not converged

W spectra peaks at around 4 dx

Linearized shallow-water equations

$$u_t = -g h_x, \quad h_t = -H u_x$$

A – grid

$$u_t = -g \ \left(h_{x+\Delta x} - h_{x-\Delta x}\right)/2\Delta x$$

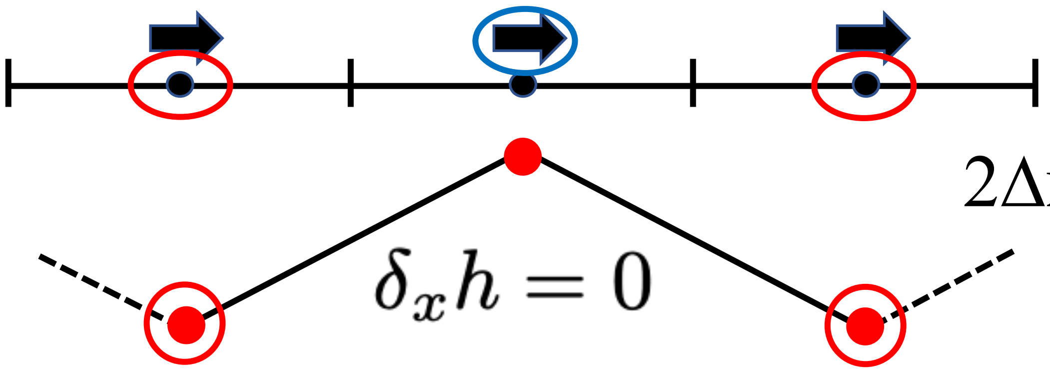

C – grid

$$u_t = -g \ \left(h_{x+\Delta x/2} - h_{x-\Delta x/2}\right)/\Delta x$$

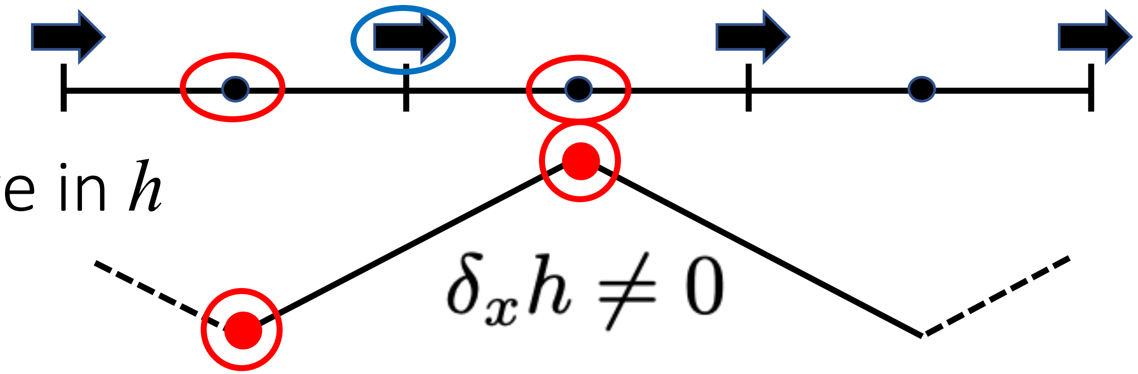

2Δx wave in h

$$h_t = -H \ \left(u_{x+\Delta x} - u_{x-\Delta x}\right)/2\Delta x$$

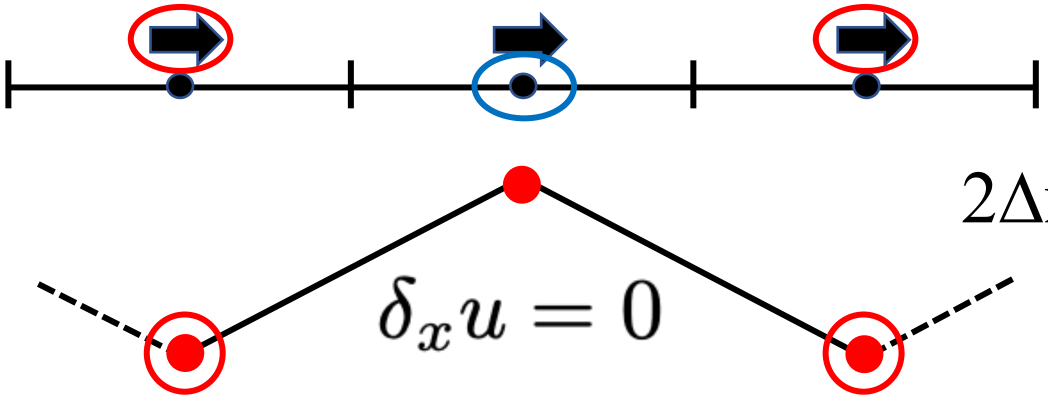

$$h_t = -H \ \left(u_{x+\Delta x/2} - u_{x-\Delta x/2}\right)/\Delta x$$

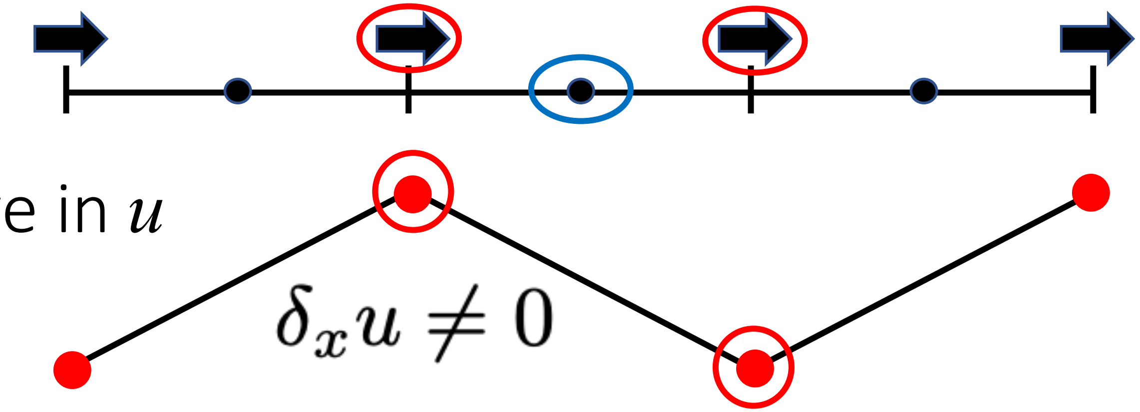

2Δx wave in u

Linearized shallow-water equations

$$u_t = -gh_x, \quad h_t = -Hu_x$$

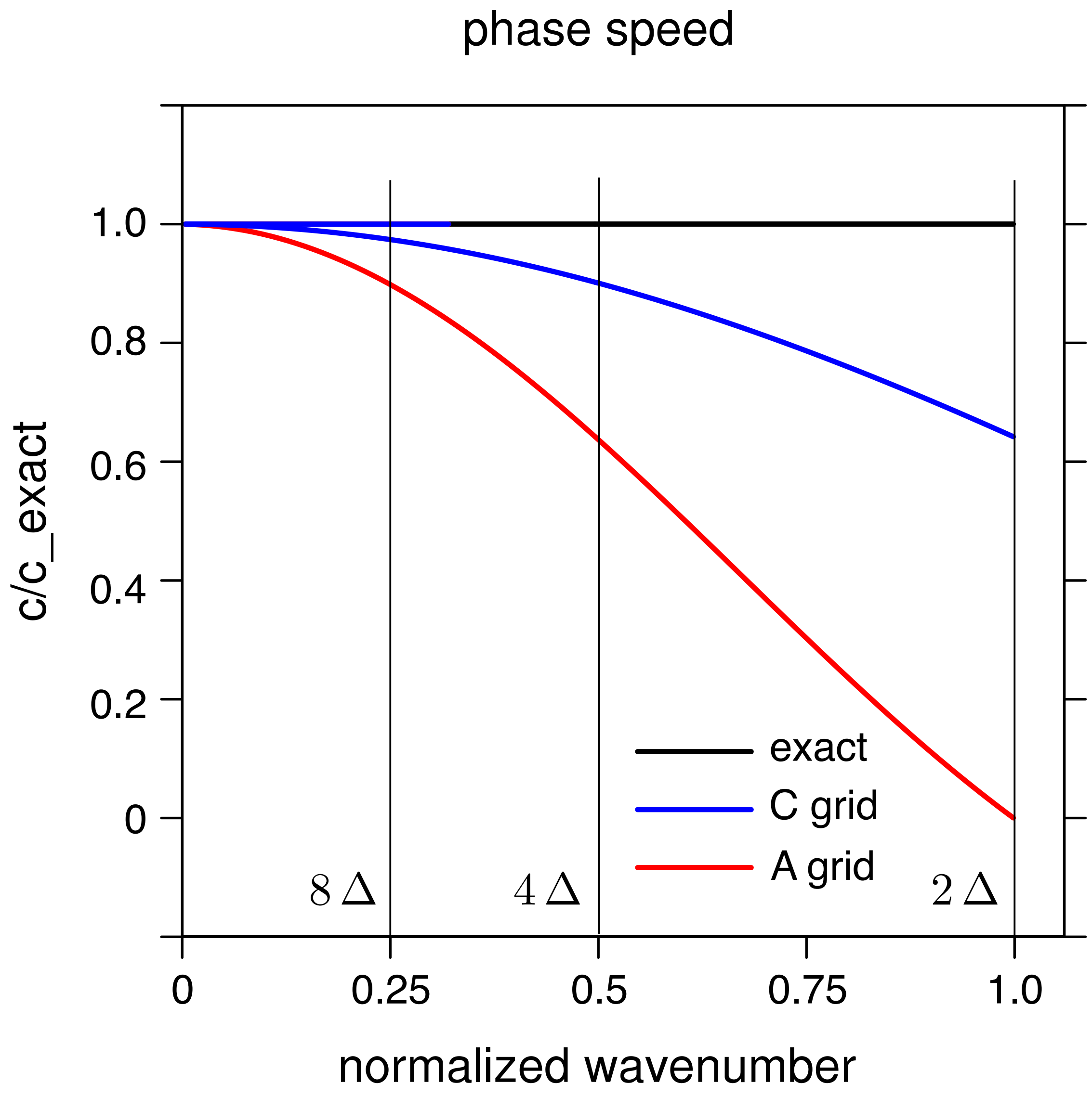

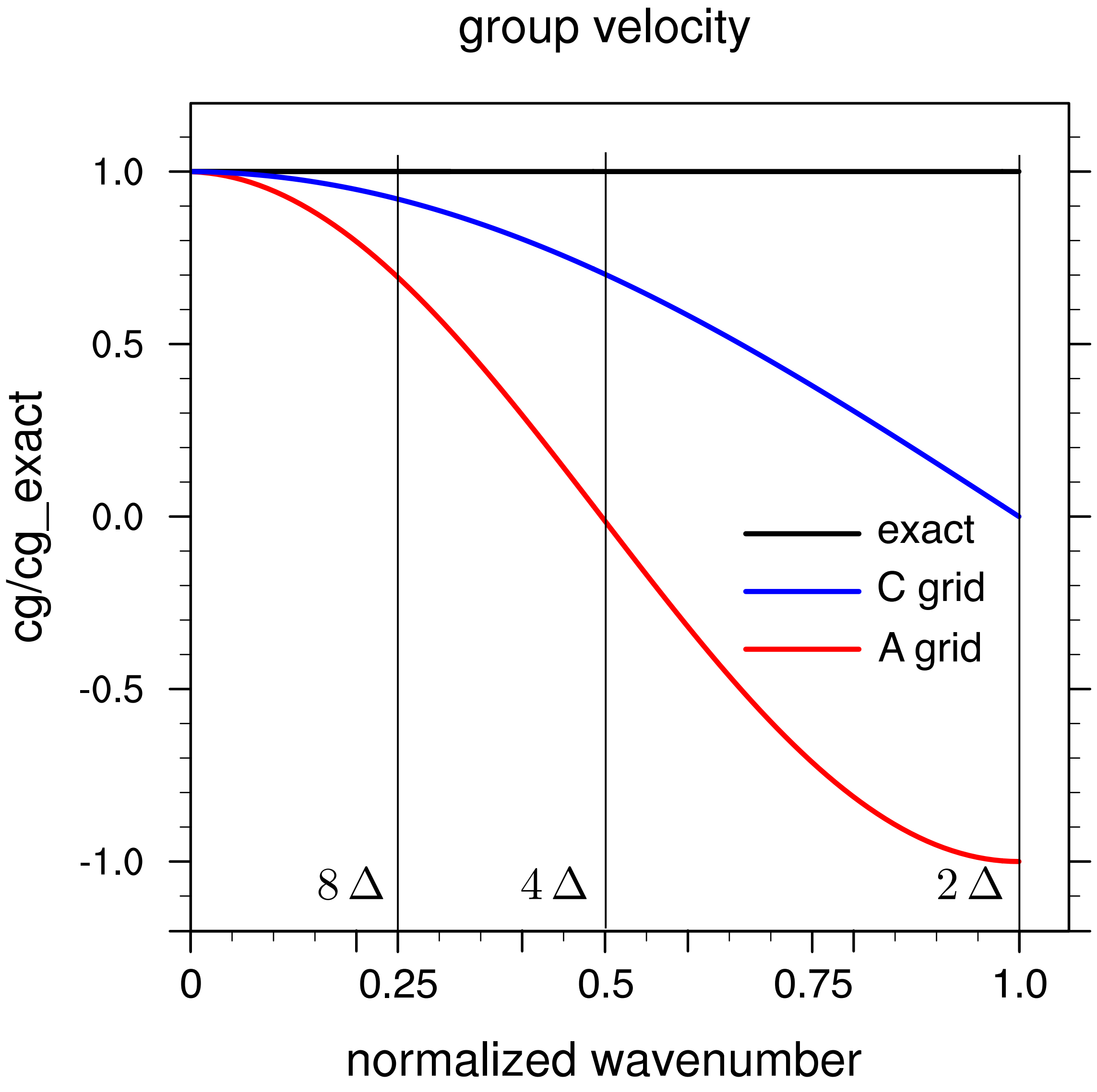

Why Use the C-Grid?

- Critical phenomena (convection) are at the margins of the mesh resolution
- C-grid has twice the effective resolution of the A-grid for divergent modes
- The timestep restriction of the C-grid can be addressed using forward-backward differencing (pressure-gradient – divergence)
- Integration cost scales as Δx^3, so using a C-grid staggering arguably produces the most *efficient* solver

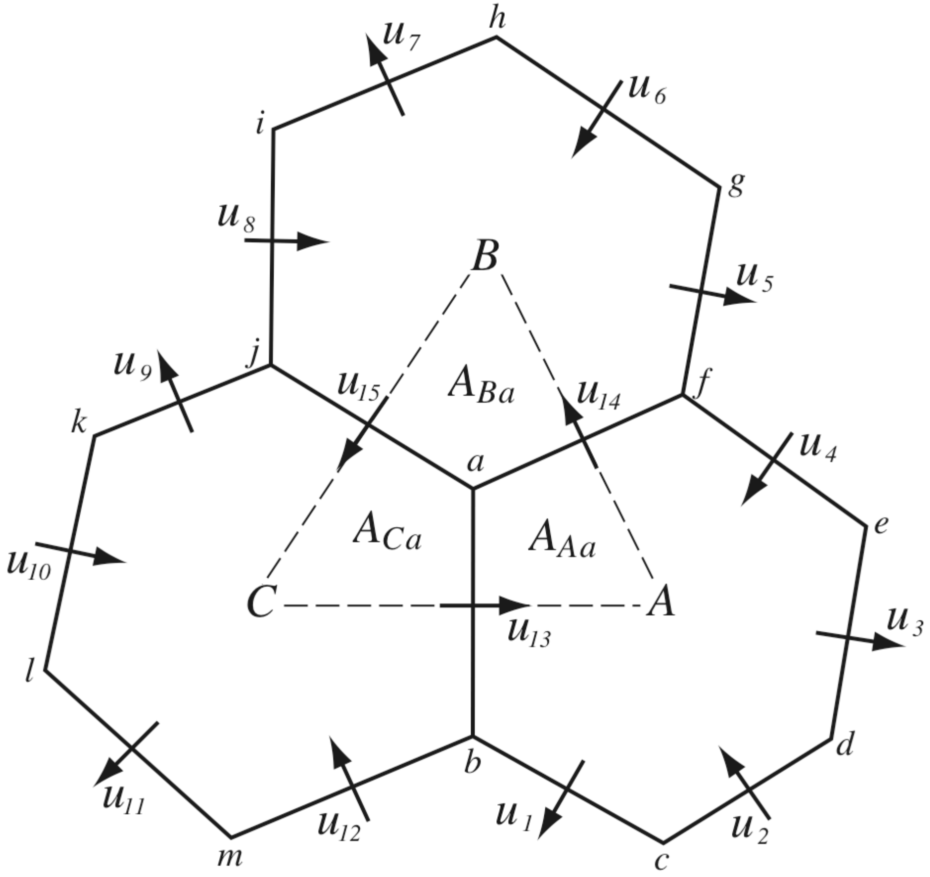

Intermission

<u>Main points from the first half</u>

Convection permitting resolution is not *convection resolving* resolution

The C-grid staggering is used in most convective-scale models because it better represents divergent motions at the margins of the resolution.

C-grids are arguably *more efficient* than other configurations for convection.

Operators on the Voronoi Mesh
'Nonlinear' Coriolis force

$$\frac{\partial \mathbf{V}_H}{\partial t} = -\frac{\rho_d}{\rho_m}\left[\nabla_\zeta\left(\frac{p}{\zeta_z}\right) - \frac{\partial \mathbf{z}_H p}{\partial \zeta}\right] - \eta \mathbf{k} \times \mathbf{V}_H - \mathbf{v}_H \nabla_\zeta \cdot \mathbf{V} - \frac{\partial \Omega \mathbf{v}_H}{\partial \zeta} - \rho_d \nabla_\zeta K - eW \cos\alpha_r - \frac{uW}{r_e} + \mathbf{F}_{V_H},$$

Linear piece $f\ \mathbf{k} \times V_H$, consider u_{13}

We need to reconstruct the tangential velocity

Simplest approach: Construct tangential velocities from weighted sum of the four nearest neighbors.

Result: Physically stationary geostrophic modes (geostrophically-balanced flow) will not be stationary in the discrete system; the solver is unusable.

(see Nickovic et al MWR 2002)

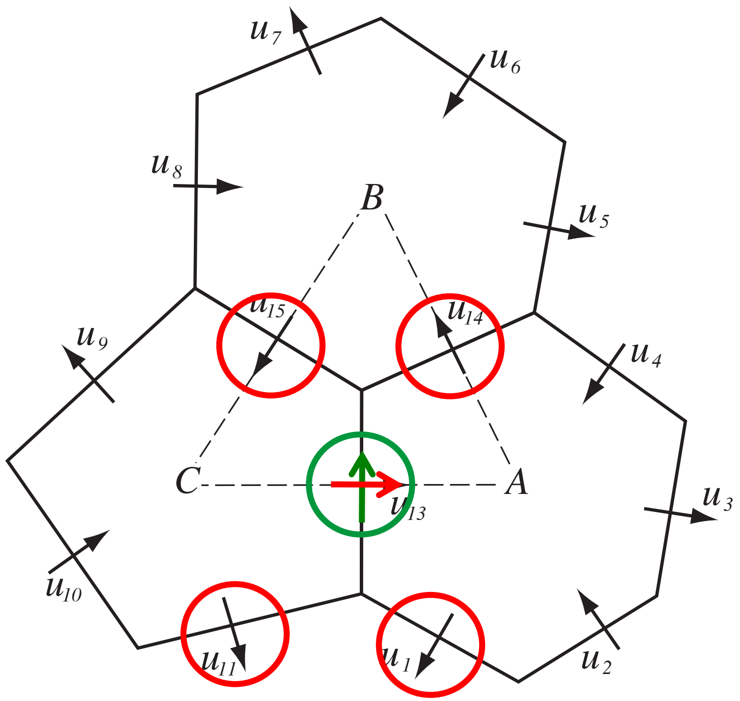

Hexagonal C-Grid Problem:
Non-Stationary Geostrophic Mode

Most obvious tangential velocity reconstruction

$$\partial_t u_1 + g\delta_{x_1} h + \frac{f}{\sqrt{3}}(u_{31} - u_{21}) = 0$$

$$\partial_t u_2 + g\delta_{x_2} h + \frac{f}{\sqrt{3}}(u_{12} - u_{32}) = 0$$

$$\partial_t u_3 + g\delta_{x_3} h + \frac{f}{\sqrt{3}}(u_{23} - u_{13}) = 0$$

$$\partial_t h + \tfrac{2}{3}H(\delta_{x_1} u_1 + \delta_{x_2} u_2 + \delta_{x_3} u_3) = 0$$

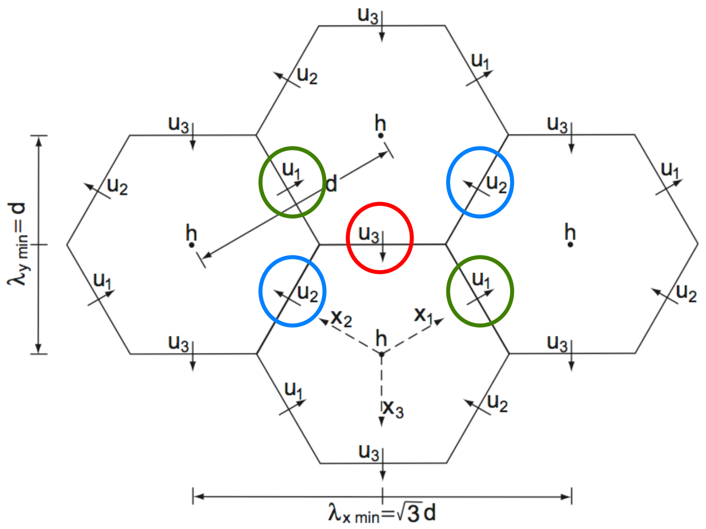

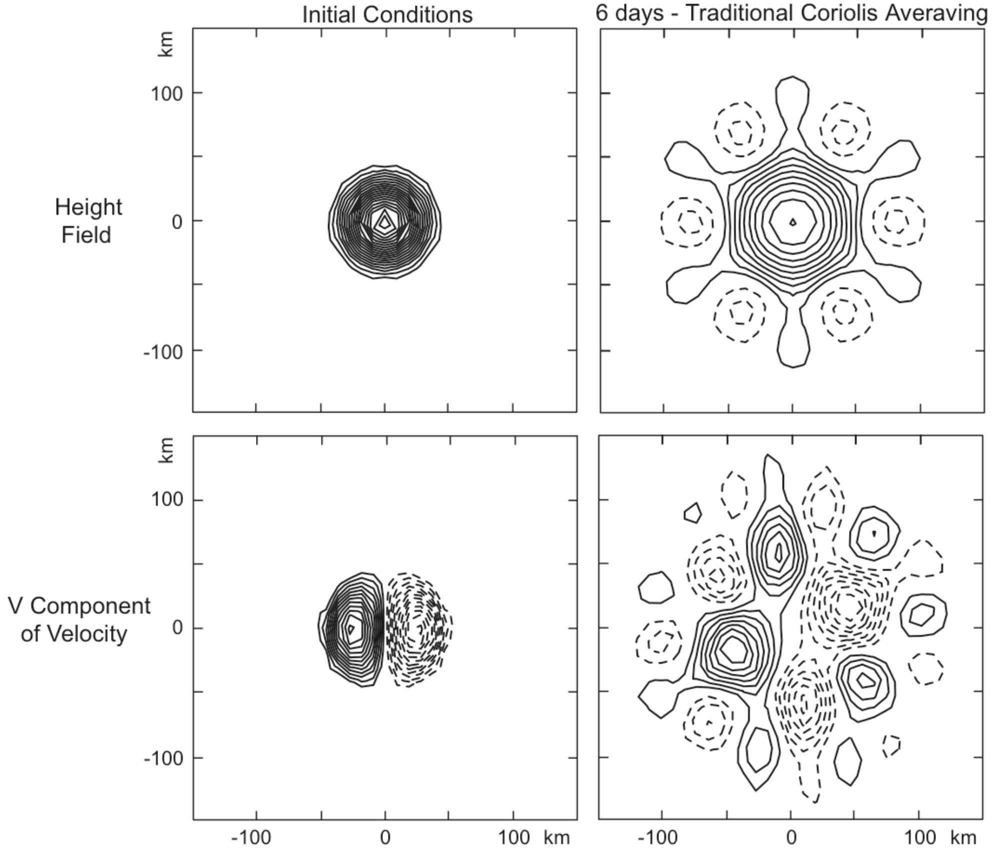

(see Nickovic et al MWR 2002)

Hexagonal C-Grid Problem: Non-Stationary Geostrophic Mode

New tangential velocity reconstruction (Thuburn, 2008 JCP)

$$\partial_t u_1 + g\delta_{x_1} h + \frac{f}{\sqrt{3}}(u_{31} - u_{21}) = 0$$
$$\partial_t u_2 + g\delta_{x_2} h + \frac{f}{\sqrt{3}}(u_{12} - u_{32}) = 0$$
$$\partial_t u_3 + g\delta_{x_3} h + \frac{f}{\sqrt{3}}(u_{23} - u_{13}) = 0$$
$$\partial_t h + \tfrac{2}{3} H(\delta_{x_1} u_1 + \delta_{x_2} u_2 + \delta_{x_3} u_3) = 0$$

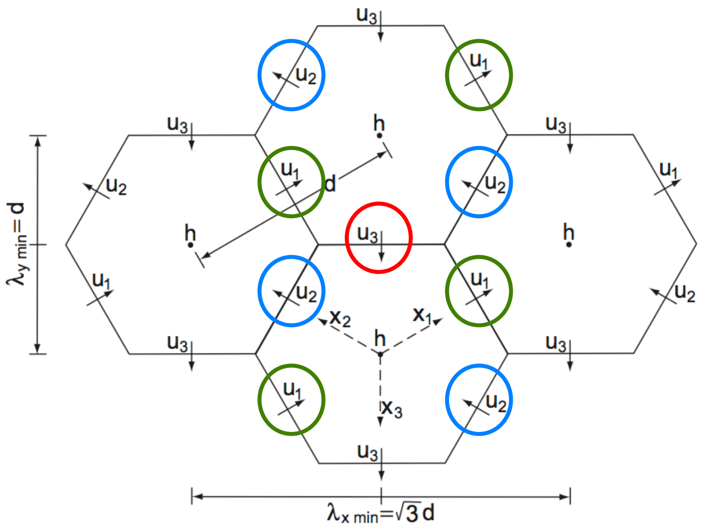

$$u_{21} = \tfrac{1}{3}\,\overline{u_2}^{x_3} + \tfrac{2}{3}\,\overline{\overline{u_2}^{x_1}}^{x_2}, \quad u_{31} = \tfrac{1}{3}\,\overline{u_3}^{x_2} + \tfrac{2}{3}\,\overline{\overline{u_3}^{x_1}}^{x_3},$$
$$u_{12} = \tfrac{1}{3}\,\overline{u_1}^{x_3} + \tfrac{2}{3}\,\overline{\overline{u_1}^{x_1}}^{x_2}, \quad u_{32} = \tfrac{1}{3}\,\overline{u_3}^{x_1} + \tfrac{2}{3}\,\overline{\overline{u_3}^{x_2}}^{x_3},$$
$$u_{13} = \tfrac{1}{3}\,\overline{u_1}^{x_2} + \tfrac{2}{3}\,\overline{\overline{u_1}^{x_1}}^{x_3}, \quad u_{23} = \tfrac{1}{3}\,\overline{u_2}^{x_1} + \tfrac{2}{3}\,\overline{\overline{u_2}^{x_2}}^{x_3}$$

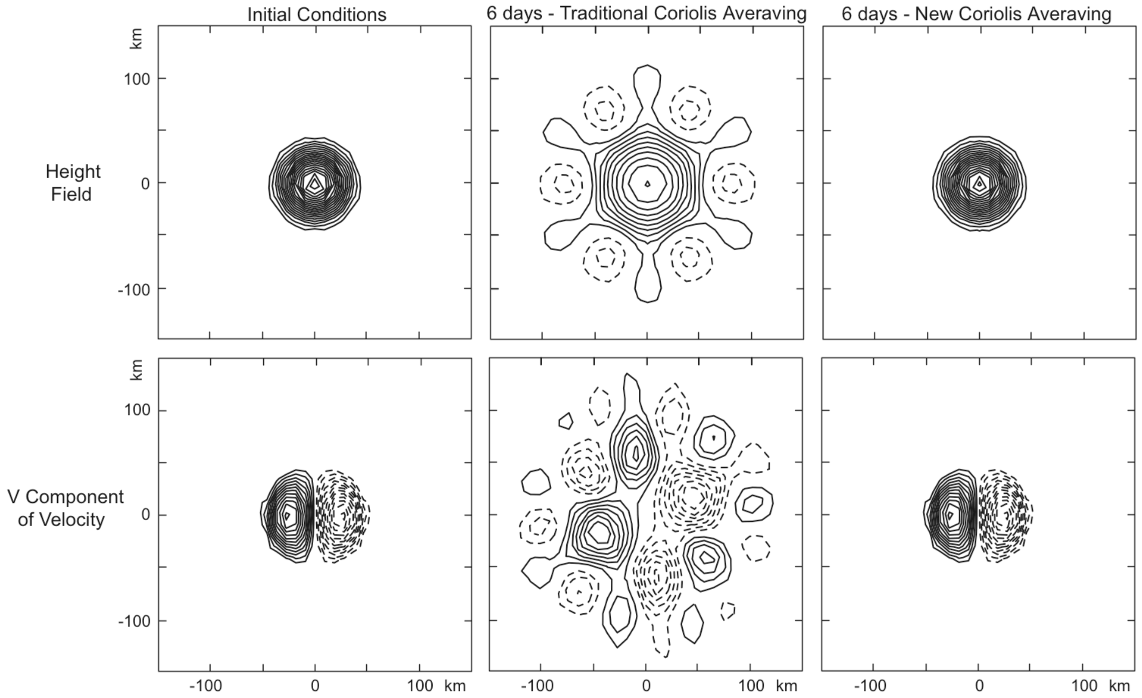

MPAS
Model for Prediction Across Scales

Operators on the Voronoi Mesh
'Nonlinear' Coriolis force

Linear piece: $f\ \mathbf{k} \times \mathbf{V}_H$

We construct tangential velocities from a weighted sum of normal velocities on edges of the adjacent cells.

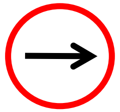

$$d_e\, u_e^{\perp} = \sum_j w_e^j\, l_j\, u_j$$

We choose the weights such that the divergence in the triangle is the area-weighted sum of the divergence in the Voronoi cells sharing the vertex.

Result: geostrophic modes are stationary; local and global mass and PV conservation is satisfied on the dual (triangular) mesh (for the SW equations).

The general tangential velocity reconstruction also allows for PV, enstrophy and energy conservation in the nonlinear SW solver.*

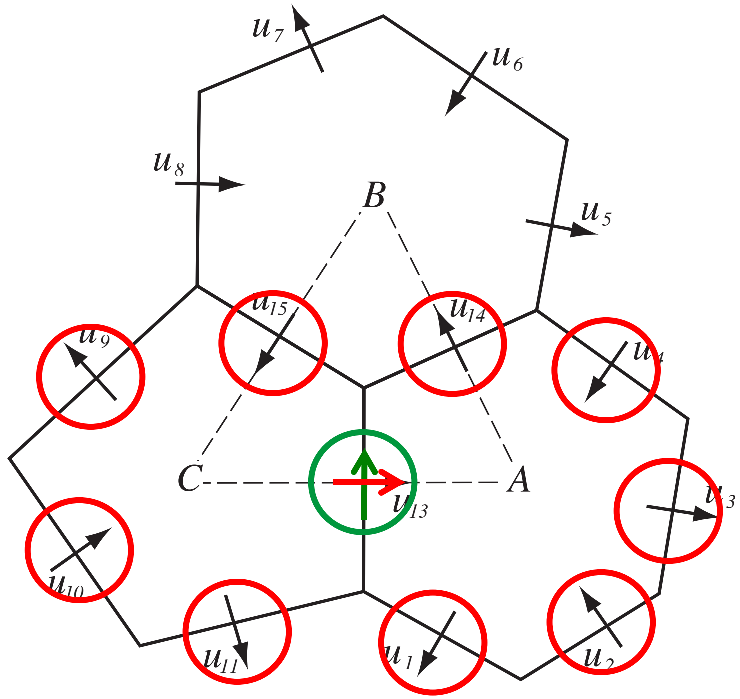

Thuburn et al (2009 JCP)
Ringler et at (2010, JCP)

MPAS
Model for Prediction Across Scales

Operators on the Voronoi Mesh
'Nonlinear' Coriolis force

Linear piece: $f\ \mathbf{k} \times V_H$

We construct tangential velocities from a weighted sum of normal velocities on edges of the adjacent cells.

$$d_e\, u_e^{\perp} = \sum_j w_e^j\, l_j\, u_j$$

We choose the weights such that the divergence in the triangle is the area-weighted sum of the divergence in the Voronoi cells sharing the vertex.

Why does this work?

Consider the linearized SW equations

$$h_t = H\, \nabla \cdot \mathbf{V}$$
$$\zeta_t = -f\, \nabla \cdot \mathbf{V}$$

Divergences on primary and dual meshes must be consistent to maintain stationarity

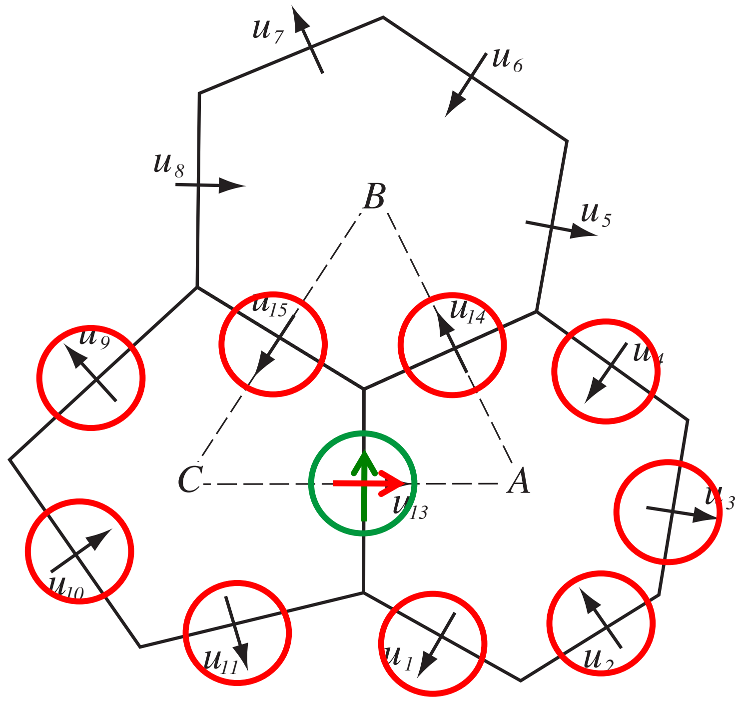

Thuburn et al (2009 JCP)
Ringler et at (2010, JCP)

Operators on the Voronoi Mesh
'Nonlinear' Coriolis force

$$\frac{\partial \mathbf{V}_H}{\partial t} = -\frac{\rho_d}{\rho_m}\left[\nabla_\zeta\left(\frac{p}{\zeta_z}\right) - \frac{\partial \mathbf{z}_H p}{\partial \zeta}\right] - \eta\,\mathbf{k}\times\mathbf{V}_H - \mathbf{v}_H \nabla_\zeta \cdot \mathbf{V} - \frac{\partial \Omega \mathbf{v}_H}{\partial \zeta} - \rho_d \nabla_\zeta K + \mathbf{F}_{V_H}$$

Tangential velocity reconstruction: $v_{e_i} = \sum_{j=1}^{n_{e_i}} w_{e_{i,j}} u_{e_{i,j}}$

Nonlinear term:

$$[\eta\,\boldsymbol{k}\times \mathbf{V}_H]_{e_i} = \sum_{j=1}^{n_{e_i}} \frac{1}{2}(\eta_{e_i} + \eta_{e_{i,j}})\, w_{e_{i,j}} \rho_{e_{i,j}} u_{e_{i,j}}$$

The general tangential velocity reconstruction produces a consistent divergence on the primal and dual grids, and allows for PV, enstrophy and energy* conservation in the nonlinear SW solver.

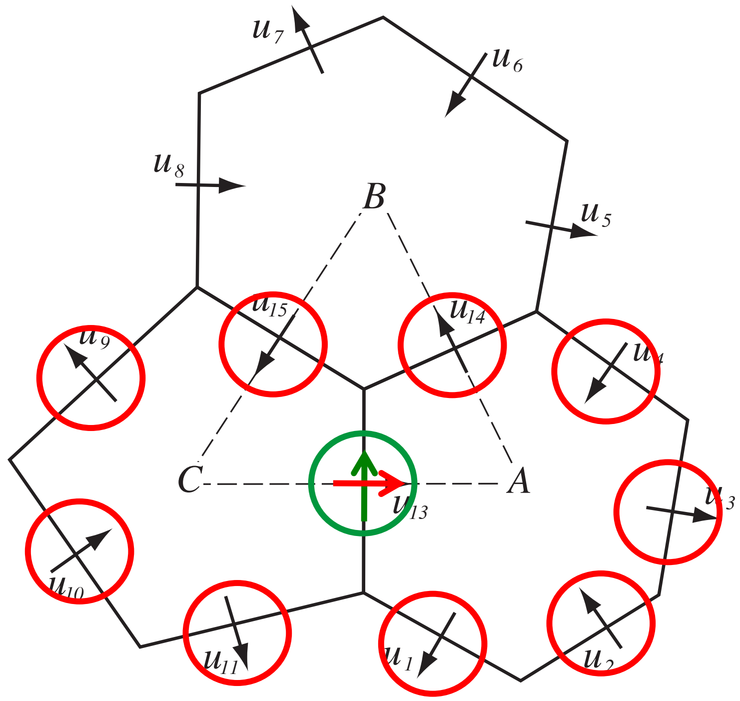

Thuburn et al (2009 JCP)
Ringler et at (2010, JCP)

MPAS
Model for Prediction Across Scales

Flux divergence, transport, and Runge-Kutta time integration

Scalar transport equation for cell *i*:

$$\frac{\partial(\rho\psi)_i}{\partial t} = L(\mathrm{V},\rho,\psi) = -\frac{1}{A_i}\sum_{n_{e_i}} d_{e_i}\left(\rho \mathrm{V}\cdot\vec{n}_{e_i}\right)\overline{\psi}$$

1. Scalar edge-flux value $\overline{\psi}$ is the weighted sum of cell values from cells that share edge and all their neighbors.
2. An individual edge-flux is used to update the two cells that share the edge.
3. Three edge-flux evaluations and cell updates are needed to complete the Runge-Kutta timestep.
4. Monotonic constraint requires checking the cell-value update and renormalizing edge-fluxes if the cell updates are outside specific bounds (on the final RK3 update).

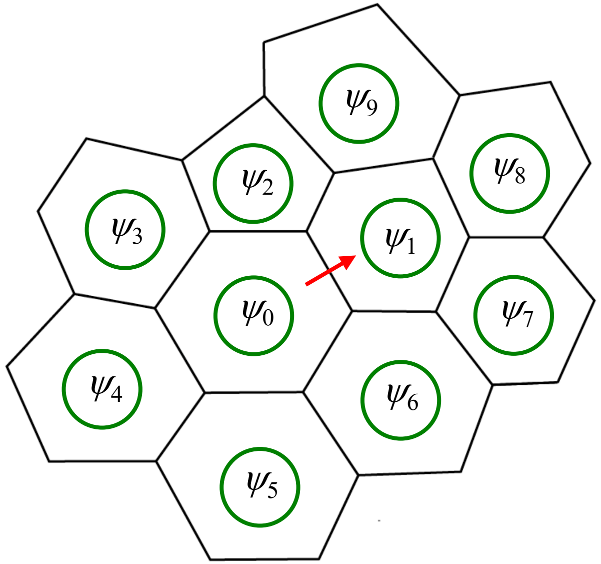

$$(\rho\psi)^{*} = (\rho\psi)^{t} + \frac{\Delta t}{3} L(\mathbf{V},\rho,\psi^{t})$$

$$(\rho\psi)^{**} = (\rho\psi)^{t} + \frac{\Delta t}{2} L(\mathbf{V},\rho,\psi^{*})$$

$$(\rho\psi)^{t+\Delta t} = (\rho\psi)^{t} + \Delta t\, L(\mathbf{V},\rho,\psi^{**})$$

(Skamarock and Gassmann, MWR 2011)

MPAS
Model for Prediction Across Scales

Conservative Transport with RK3 Time Integration: *Examples*

- The quality of solutions for convection-permitting integrations is strongly dependent on the transport schemes for scalars employed in the solver.
- We employ flux operators similar to those used in WRF but adapted to the unstructured Voronoi mesh using least-squares fit polynomials.

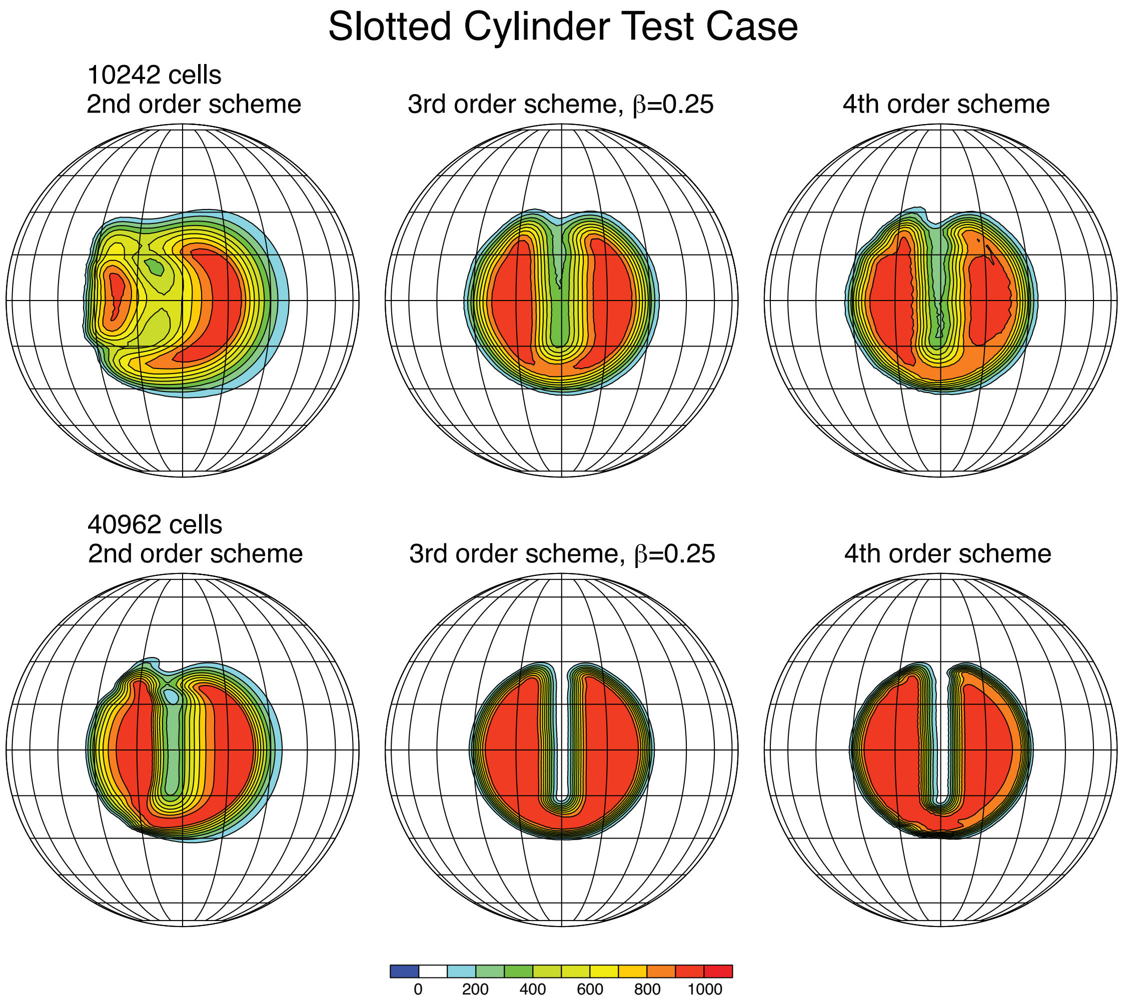

Solid-body rotation, 1 revolution around the sphere

(Skamarock and Gassmann, MWR 2011)

Model for Prediction Across Scales

Conservative Transport with RK3 Time Integration: *Examples*

163842 cells, ~ 60 km cell spacing (~ 1/2 deg), Cr max ~ 0.8

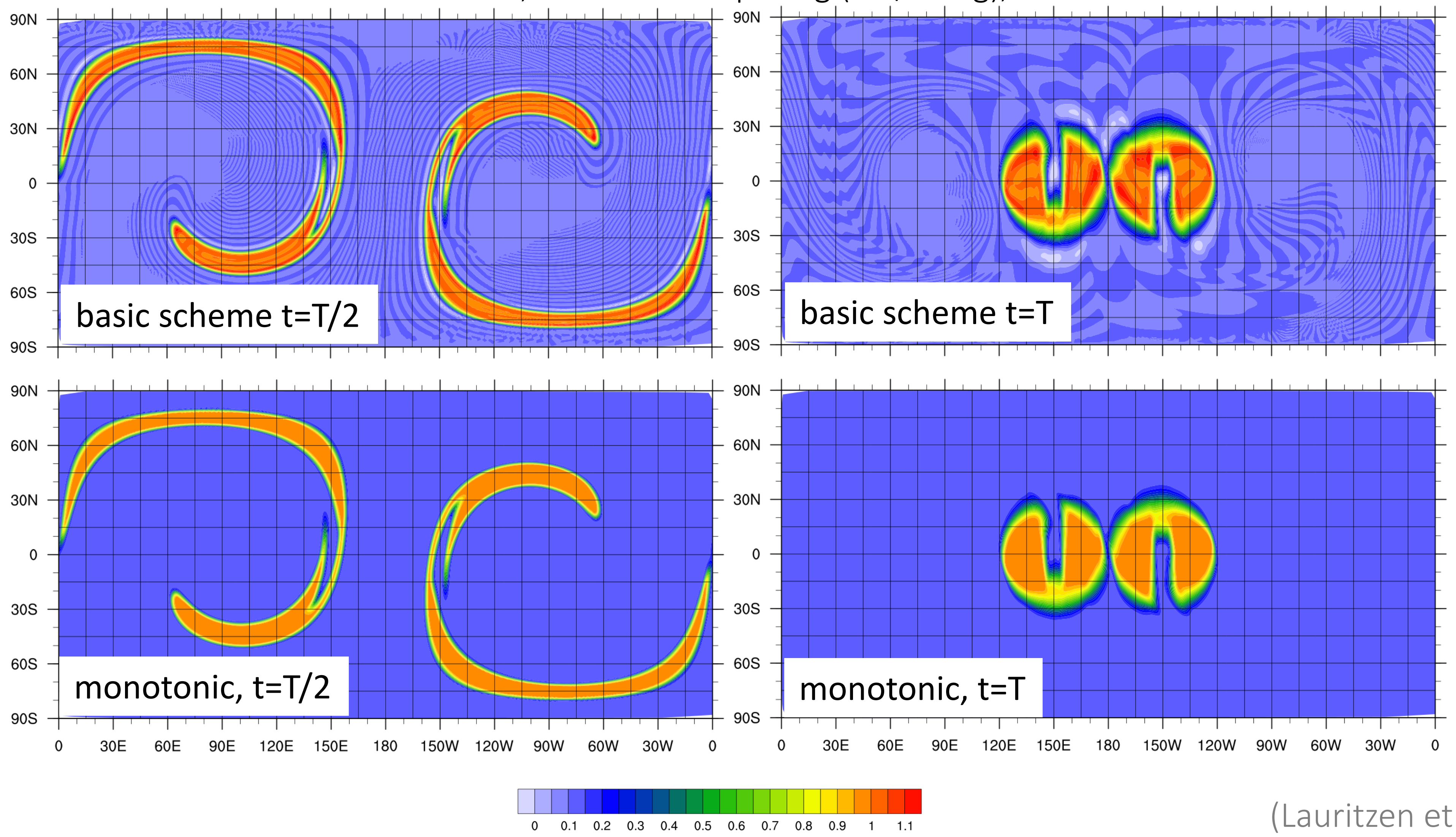

(Lauritzen et al, GMD 2014)

MPAS

Model for Prediction Across Scales

MPAS Vertical Mesh

Specification of terrain:

- High resolution terrain data (30 arcsec) averaged over grid-cell area
- Terrain smoothing with one pass of a 4th order Laplacian

Smoothed Terrain-Following (STF) hybrid Coordinate

$$z(x, y, \zeta) = \zeta + A(\zeta) h_s(x, y, \zeta)$$

$A(\zeta)$ Controls rate at which terrain influences are attenuated with height

$h_s(x, y, \zeta)$ Terrain influence that represents increased smoothing of the actual terrain with height

Multiple passes of simple Laplacian smoother at each ζ level:

$$h_s^{(n)} = h_s^{(n-1)} + \beta(\zeta) d^2 \nabla_\zeta^2 h_s^{(n-1)}$$

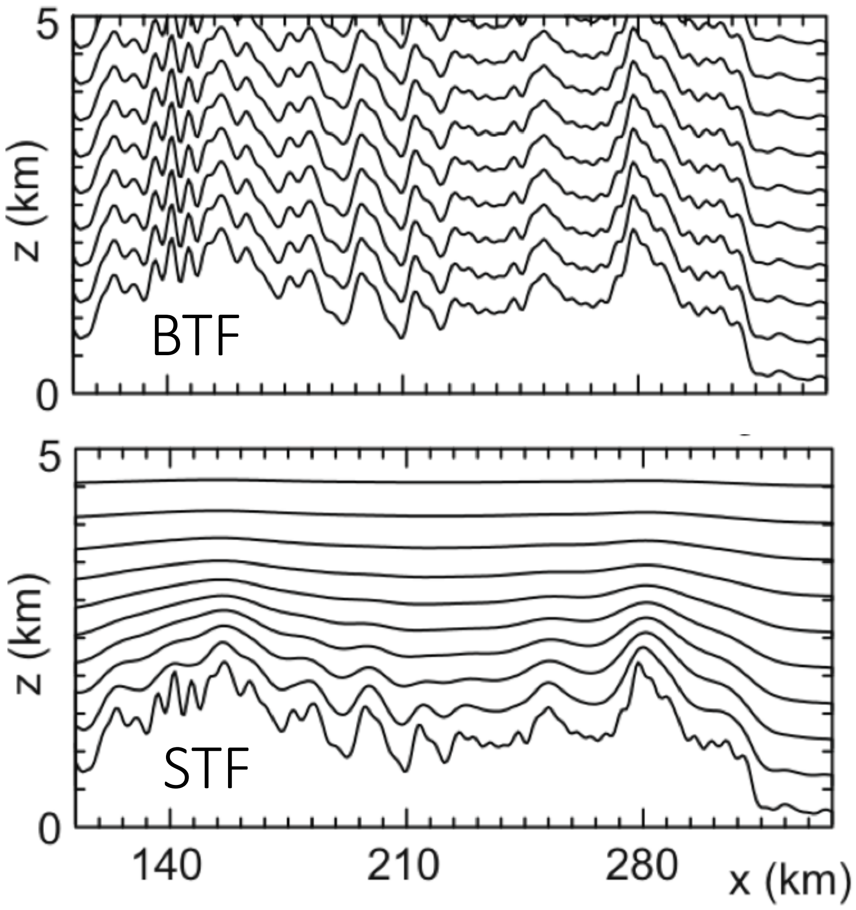

STF progressively smooths coordinate surfaces while transitioning to a height coordinate

MPAS -Tibetan Plateau, 28^o N

MPAS
Model for Prediction Across Scales

Smoothed hybrid terrain-following (STF) coordinate

(Model top is at 30 km)

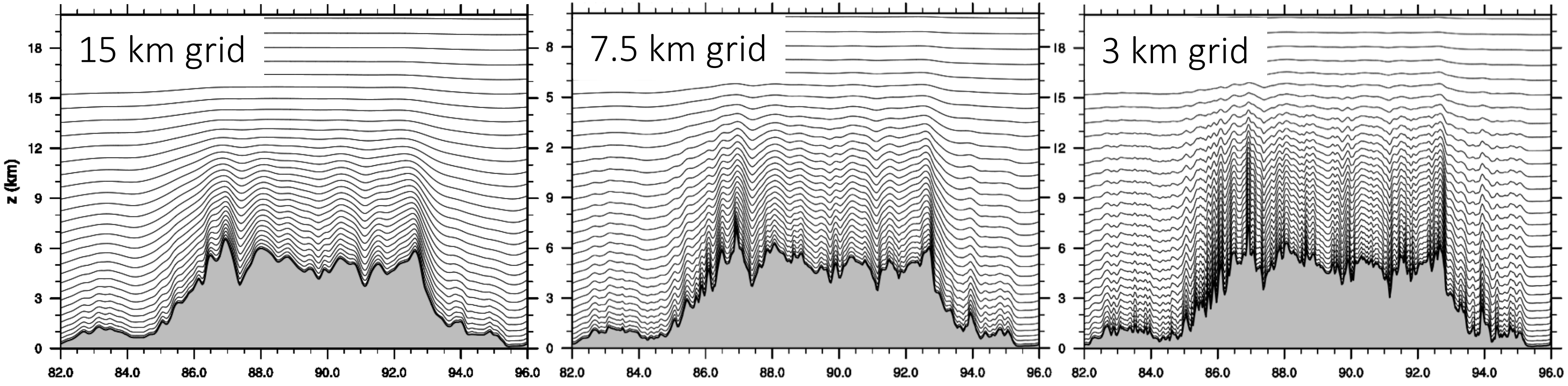

Basic terrain-following (BTF) coordinate

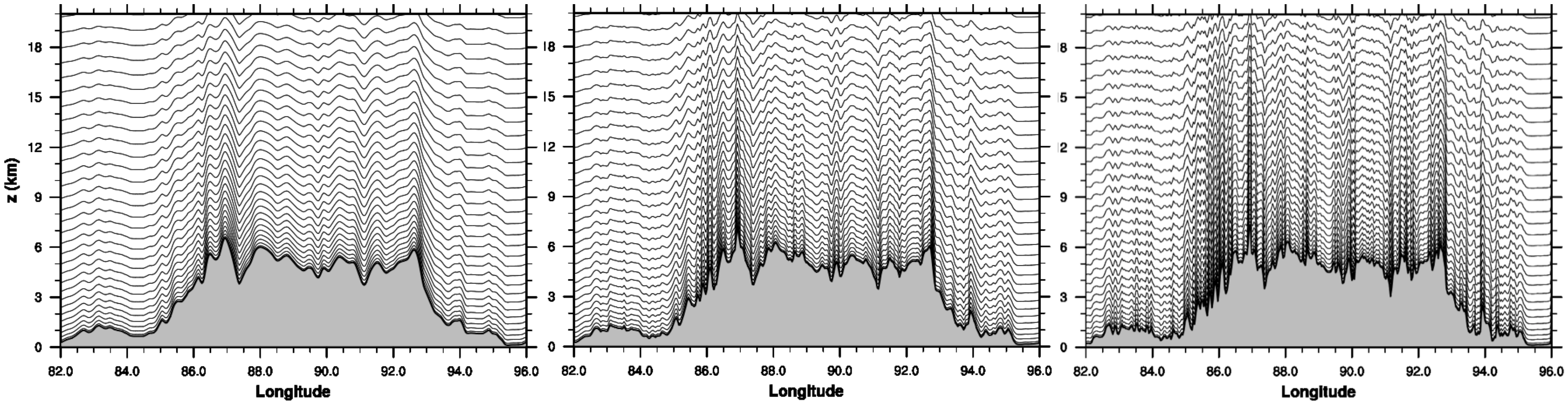

MPAS
Model for Prediction Across Scales

Atmospheric Convection and MPAS

MPAS was designed to simulate atmospheric convection with fidelity similar to state-of-the-art cloud models.

At what mesh spacing does MPAS reproduce observed convective structures?

Midlatitude convection:
3 km mesh spacing.

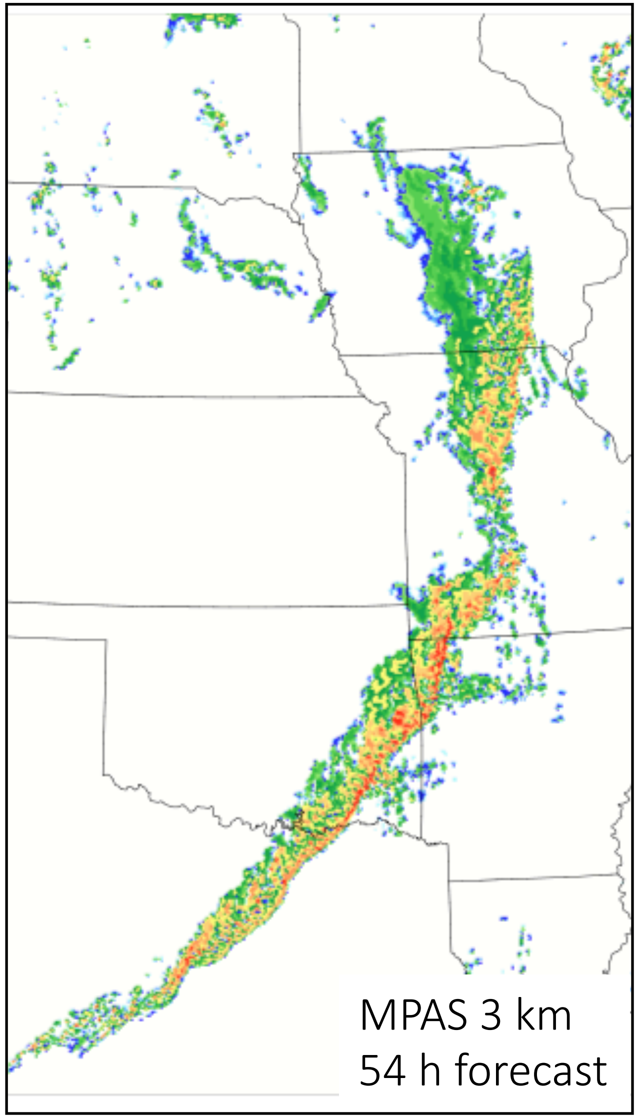

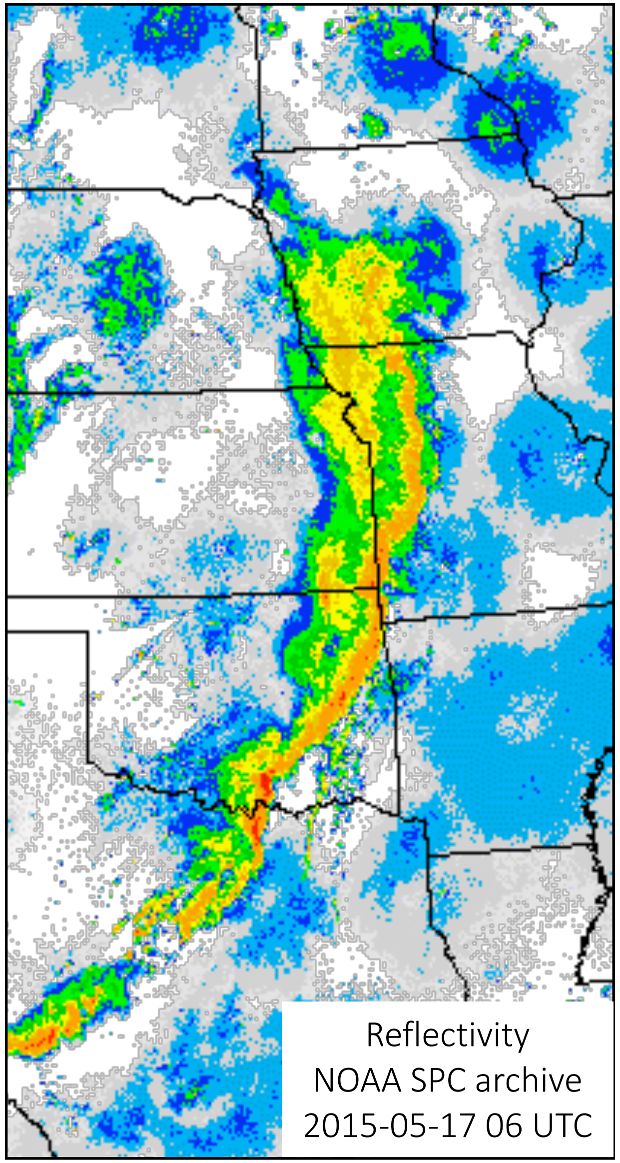

MPAS
Model for Prediction Across Scales

The MPAS SCVT approach

Strengths

- Convection-permitting simulations
- Flexibility
  - global
  - regional
  - variable-resolution
  - 2D and 3D Cartesian planes
- Conservation properties
- Explicit solver is easy to configure
- Solver scales well, easily adaptable to accelerators (GPUs)

Weaknesses

- Mesh generation is very expensive
- Novelty of an unstructured mesh
  - Standard pre- and post-processors are not unstructured-mesh friendly
- Perceived high integration cost
  - More than balanced by increased accuracy at convection–permitting resolutions (?)